

INVESTIGATION INTO THE EXTRUSION OF POROUS METAL USING FINITE ELEMENT METHOD

UDC 669-126:519.6

Summary

Powder forming is particularly attractive because it allows cost and material saving advantages of conventional powder metallurgy, as well as high production rates and property enhancement by forming. Therefore, powder forming is now a viable commercial method for the fabrication of high-strength parts. This study applied the finite element method to investigate deformation behaviour and density variation in extrusions of porous metal. Effects of parameters such as reduction of area, die semi-angle, initial relative density and friction factor on extrusion force, effective stress distribution, relative density variation and inhomogeneous factor are also examined.

Key words: extrusion, porous metal, finite element method.

1. Introduction

In the powder extrusion process, the essential requirement is a uniform distribution of high relative density within final products. This is because the region of non-uniform or/and lower density distribution may trigger the failure of products. Therefore, understanding the deformation behaviour and the density distribution of porous metals during forming is very important in achieving good quality powder metallurgy parts.

Khoei et al. [1] used an adopted finite element approach which is characterized by the use of the penalty approach in which a plasticity theory of friction is incorporated to simulate sliding resistance at the powder-tool interface. The frictional contact formulation is performed within the framework of the large FE deformation in order to predict the non-uniform relative density distribution during the large deformation of powder die pressing. Liao [2] shows the simulation results that demonstrate that the yield function of the corresponding matrix plays an important role both on the strain distribution and the strain localization. Yang and Hsu [3] used the DEFOM-2D software to simulate the forging force and the porosity variation of the porous metal in upsetting. The results show good agreement with experimental data of Huang and Cheng [4].

Forward extrusion is a forming process in which a workpiece is pushed through a die whose exit diameter is smaller than that of the workpiece. In this paper, a finite element method is used to investigate the deformation behaviour and density variation of the extrusion of porous metal. The effects of the process parameters on force, effective stress, effective strain and relative density distributions during the extrusion of porous metal are also examined.

2. Basic theory

2.1 Finite Element Modelling

This study applies the commercial FEM DEFORM-2D [5] to simulate the plastic deformation behaviour during the extrusion process. The basic equations of the rigid-plastic finite element are as follows:

Equilibrium equation:

$$\sigma_{ij,j} = 0, \quad (1)$$

Compatibility and incompressibility equations:

$$\dot{\epsilon}_{ij} = \frac{1}{2}(u_{i,j} + u_{j,i}), \quad \dot{\epsilon}_v = u_{i,i} = 0, \quad (2)$$

Constitutive equations:

$$\sigma'_{ij} = \frac{2\bar{\sigma}}{3\bar{\epsilon}}\dot{\epsilon}_{ij}, \quad \bar{\sigma} = \sqrt{\frac{3}{2}(\sigma'_{ij}\sigma'_{ij})}, \quad \bar{\epsilon} = \sqrt{\frac{3}{2}(\dot{\epsilon}_{ij}\dot{\epsilon}_{ij})}, \quad (3)$$

Boundary conditions:

$$\sigma_{ij}n_i = F_j \quad \text{on } S_F, \quad u_i = U_i \quad \text{on } S_U, \quad (4)$$

where σ_{ij} and $\dot{\epsilon}_{ij}$ are the stress and the strain rate, respectively, $\bar{\sigma}$ and $\bar{\epsilon}$ are the effective stress and the effective strain rate, respectively, F_j is the force on the boundary surface of S_F , and U_i is the deformation velocity on the boundary surface of S_U . The weak form of the rigid-plastic FEM can be determined by applying the variational method to Eqs. (1)-(4), i.e.

$$\int \left(\frac{2\bar{\sigma}}{3\bar{\epsilon}} \right) \dot{\epsilon}_{ij} \delta \dot{\epsilon}_{ij} dV + \int K \dot{\epsilon}_{kk} \delta \dot{\epsilon}_{ii} dV - \int_{S_F} F_i \delta u_i dS = 0, \quad (5)$$

where V and S are the volume and the surface area of material, respectively. K is the penalty constant. In the simulations, the equations are solved using the Newton-Raphson iteration method.

2.2 Plasticity Theory for Porous Metals

The onset of plastic deformation in porous metals is governed by yield criteria and flow rules that are fundamentally different from those for fully dense materials. This is due to the fact that a significant change in porosity is accompanied by volumetric strain in porous metals. A suitable yield criterion and stress-strain relationship for porous solids was expressed as [6]:

$$f'\bar{\sigma} = \left\{ \left[(\sigma_1 - \sigma_2)^2 + (\sigma_2 - \sigma_3)^2 + (\sigma_3 - \sigma_1)^2 \right] / 2 + (\sigma_m/f)^2 \right\}^{1/2}, \quad (6)$$

where f represents the degree of influence of the hydrostatic stress component, σ_m , on the onset of yielding of porous bodies and may be a function of relative density, and f' is the ratio of the apparent stress applied to the porous solid and the effective stress exerted on the metal matrix. From Eq. (6), the following stress-strain relationships can be derived:

$$d\varepsilon_i = \frac{3}{2} \frac{\rho}{f'^2} \frac{d\bar{\varepsilon}}{\bar{\sigma}} \left\{ \sigma_i - \left(1 - \frac{2}{9f^2} \right) \sigma_m \right\} ,, \quad \text{for } i=1,2,3 \quad (7)$$

where

$$d\bar{\varepsilon} = \frac{f'}{\rho} \left\{ \frac{2}{9} \left[(d\varepsilon_1 - d\varepsilon_2)^2 + (d\varepsilon_2 - d\varepsilon_3)^2 + (d\varepsilon_3 - d\varepsilon_1)^2 + (fd\varepsilon_v)^2 \right] \right\}^{1/2} ,, \quad (8)$$

and

$$d\varepsilon_v = d\varepsilon_1 + d\varepsilon_2 + d\varepsilon_3 ,, \quad (9)$$

In the above equations, $\bar{\sigma}$ and $\bar{\varepsilon}$ refer to the effective stress and the cumulative effective strain, respectively. In cold forging of spur gears, due to strain-hardening effects, the deforming material can be characterized by a relationship which provides $\bar{\sigma}$ as a function of $\bar{\varepsilon}$. The factors f and f' are, in general, functions of the relative density, ρ . For sintered porous metals, Shima and Oyane [6] suggested correlations of the form:

$$f = \frac{1}{A(1-\rho)^B} ,, \quad (10)$$

and

$$f' = \rho^C ,, \quad (11)$$

where A , B and C are the material constants. The details to determine the constants A , B and C are stated in Shima and Oyane [6]. The flow stress of the fully dense matrix of copper is shown in Figure 1.

3. RESULTS AND DISCUSSION

Yang and Hsu [3] verified that the DEFORM-2D software is sufficiently accurate for simulating porous metal forming processes. Thus, DEFORM-2D can be used to investigate the deformation behaviour and density variation of porous metal extrusions. The schematic diagram of the forward extrusion of sintered metal powder is shown in Figure 2. The dimensions of the die and the billet are shown in Figure 3. The billets are compacted and sintered by copper powders of varying initial densities. The analysis assumes that the die, container and punch are rigid and that the billet is composed of a porous material. The billet radius is 15 mm. The FE model for the extrusion of porous metal simulated in DEFORM-2D is shown in Figure 4. The billet is modelled using four-node elements in the simulation; 3400 nodes and 8800 elements were meshed. Because of symmetry, only a half of the die and the billet were taken for simulation. The friction factor is assumed 0.01 at the interfaces of the punch/billet and die/billet for good lubricated condition. The punch moves toward the billet with the same velocity of 1 mm/s. The integration scheme is of an implicit type, and its total step number is 500 (0.1 mm per step). Figures 4 (a-c) shows the initial, middle and final stage of the extrusion process of porous metal, respectively.

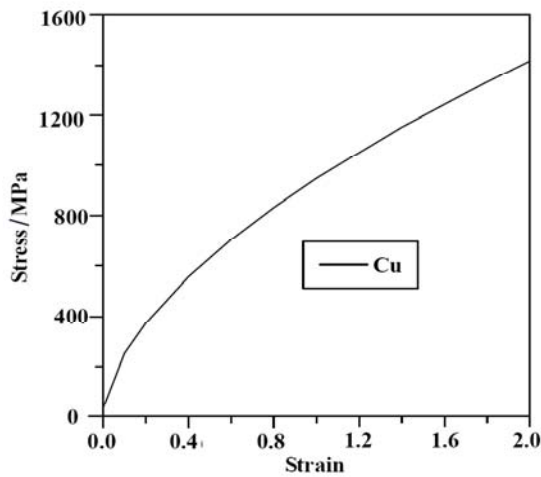


Fig. 1 Flow stress of copper

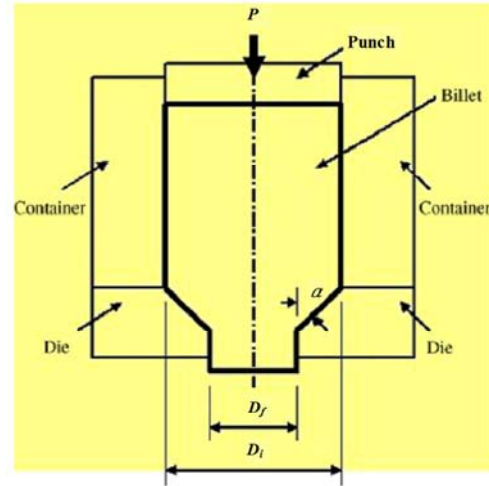


Fig. 2 Schematic of forward extrusion process

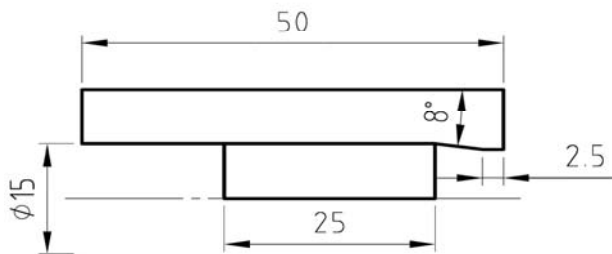
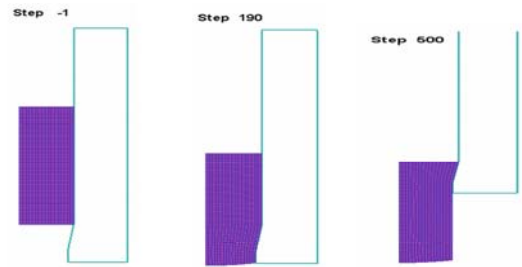


Fig. 3 Dimension of die and billet (axial symmetry)



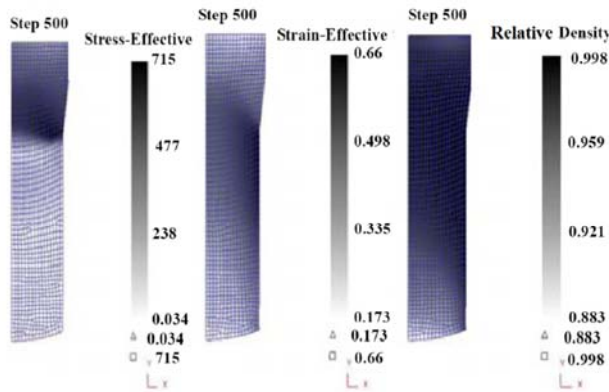
(a) initial stage (b) middle stage (c) final stage

Fig. 4 FEM model of extrusion process

Figure 5 shows the effective stress, effective strain and relative density distributions of the porous metal extrusions. The value of effective stress, effective strain and relative density at the exit portion is larger than in other regions, and the value of effective stress, effective strain and relative density increase as the distance from the centre increases. The maximum effective stress, effective strain and relative density are about 715 MPa, 0.66 and 0.998, respectively. Lin et al. [7] defined the inhomogeneity factor of effective strain IF_ϵ as:

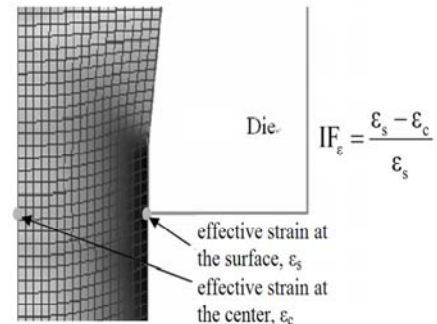
$$IF_\epsilon = \frac{\epsilon_s - \epsilon_c}{\epsilon_s} \quad (12)$$

where ϵ_s and ϵ_c are the effective strain at the surface and centre, respectively. A larger IF_ϵ represents a larger dissimilarity between the effective strain of the surface and the centre. Figure 6 shows the schematic diagram of the inhomogeneous factor of effective strain. Process variables, including the reduction of area, the semi-die angle, and the initial density were evaluated in terms of effects on the forming load, effective stress, relative density distribution and the inhomogeneity of effective strain in the extrusion of porous metal. Numerical analyses of the effects of the process variables were performed by the DEFORM-2D software. The IF was measured at the centre of each specimen.



(a) effective stress (b) effective strain (c) relative density

Fig. 5 Effective stress, strain and density distribution



IF_{ϵ} : inhomogeneous factor of effective strain

Fig. 6 Schematic diagram of inhomogeneous factor of effective strain

Figure 7 shows the effect of the reduction in area on the forming load for a semi-die angle of 8° , an initial relative density of 0.8 and a friction factor of 0.3. An increased reduction in area increases the forming load needed to extrude the porous metal. The maximum forming load values are approximately 10500 N, 39500 N and 78000 N for $R = 10\%$, 20% and 30% , respectively. Figure 8 shows the effect of the reduction in area on the effective stress distribution. The effective stress correlates with the distance from the centre and varies in ranges of 120-370 MPa, 230-550 MPa and 400-710 MPa for $R = 10\%$, 20% and 30% , respectively. Figure 9 shows the effect of the reduction in area on the effective strain distribution. The effective strain, which also correlates with the distance from the centre, varies in ranges of 0.09-0.25, 0.25-0.41 and 0.49-0.61 for $R = 10\%$, 20% and 30% , respectively. Figure 10 shows how the reduction in area affects the relative density distribution. The relative density increases as the distance from the centre increases. The relative density varies in the range of 0.86-0.95, 0.93-0.98 and 0.985-0.995 for $R = 10\%$, 20% and 30% , respectively. Table 1 shows the effect of the reduction in area on the inhomogeneous factor of effective strain. The inhomogeneity of the effective strain correlates negatively with the reduction in area.

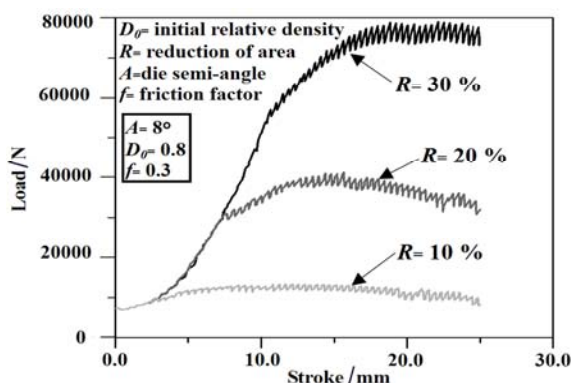


Fig. 7 Effect of reduction in area on extrusion force

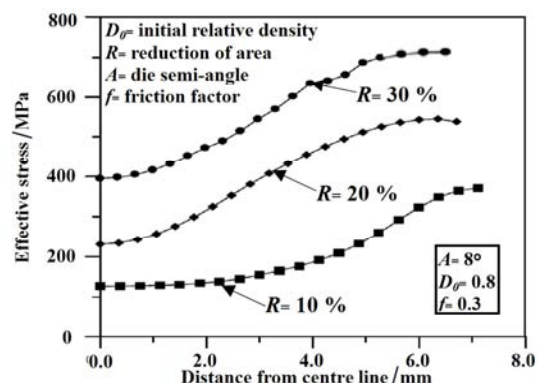


Fig. 8 Effect of reduction in area on effective stress distribution

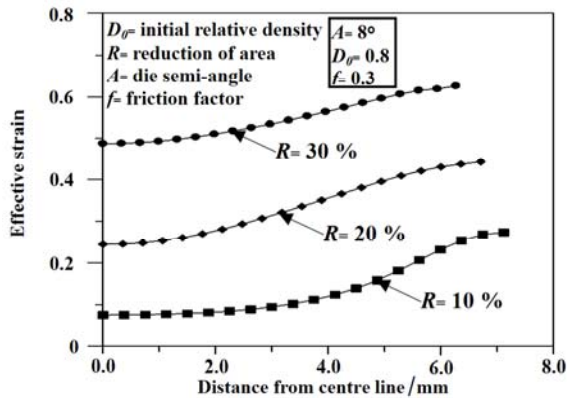


Fig. 9 Effect of reduction of area in effective strain distribution

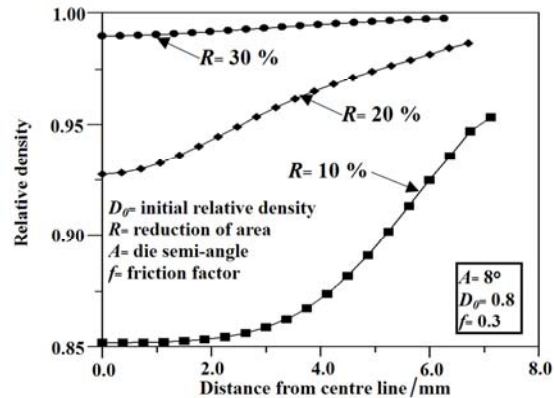


Fig. 10 Effect of reduction in area on relative density distribution

Table 1 Effect of reduction in area on the inhomogeneous factor of effective strain

Reduction	10 %	20 %	30 %
ϵ_c	0.09	0.25	0.49
ϵ_s	0.25	0.41	0.61
IF _{strain}	64.00 %	39.02 %	19.67 %

Figure 11 shows how the die semi-angle A affects the forming load under the conditions of the area reduction of 20%, the initial relative density of 0.8 and the friction factor of 0.3. A larger value of the die semi-angle would require more forming load to extrude porous metal. The maximum forming loads approximate 31000 N, 39500 N and 46000 N for $A = 4^\circ$, 8° and 12° , respectively. Figure 12 shows how the die semi-angle affects the effective stress distribution. The effective stress increases as the distance from the centre increases. The effective stress varies in the range of 290–450 MPa, 230–550 MPa and 250–630 MPa for $A = 4^\circ$, 8° and 12° , respectively. Figure 13 shows the effect of die semi-angle on the effective strain distribution. The effective strain correlates positively with the distance from the centre and varies in ranges of 0.23–0.34, 0.235–0.44 and 0.23–0.55 for $A = 4^\circ$, 8° and 12° , respectively. Figure 14 shows the effect of the die semi-angle on the relative density distribution. The relative density increases as the distance from the centre increases and varies in ranges of 0.946–0.972, 0.928–0.986 and 0.916–0.995 for $A = 4^\circ$, 8° and 12° , respectively. Table 2 shows the effect of the die semi-angle on the inhomogeneous factor of effective strain. The values of the inhomogeneous factor of effective strain increase as the die semi-angle increases.

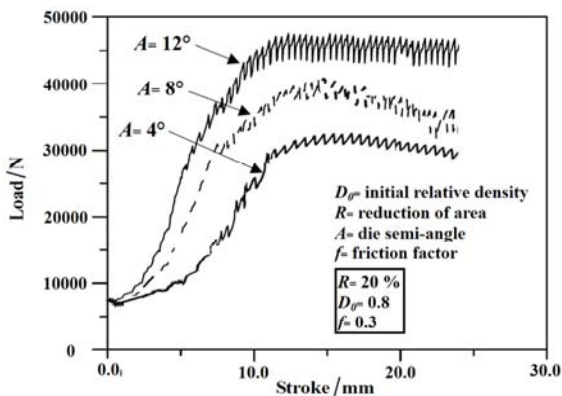


Fig. 11 Effect of die semi-angle on extrusion force

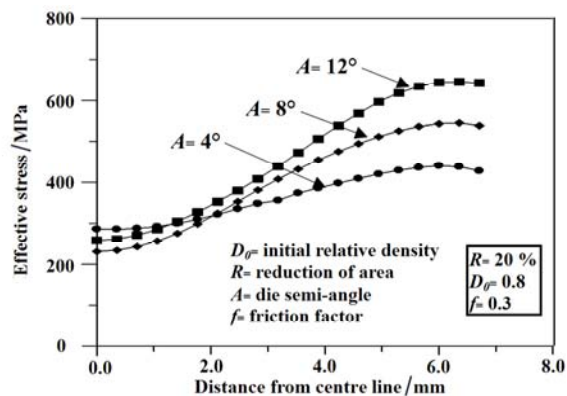


Fig. 12 Effect of die semi-angle on effective stress distribution

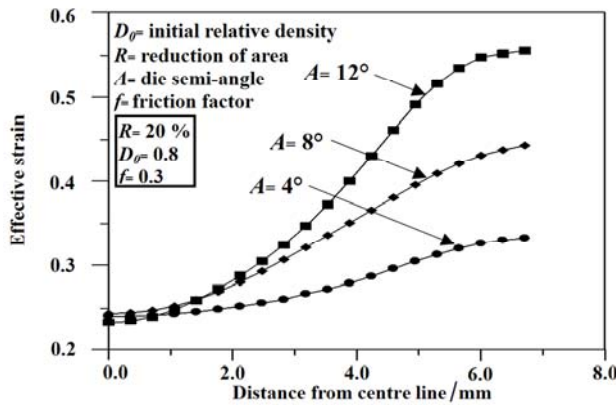


Fig. 13 Effect of die semi-angle on effective strain distribution

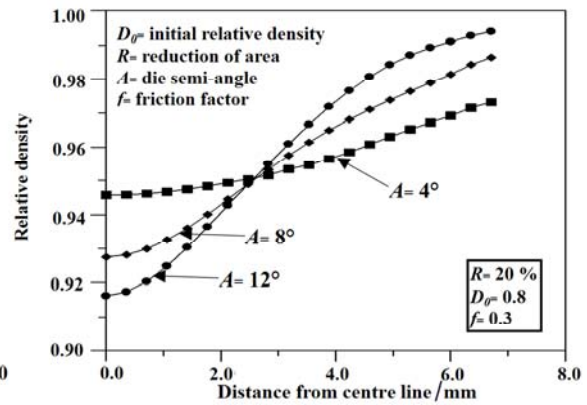


Fig. 14 Effect of die semi-angle on relative density distribution

Table 2 Effect of die semi-angle on the inhomogeneous factor of effective strain

Die semi-angle	4°	8°	12°
ϵ_c	0.23	0.235	0.23
ϵ_s	0.34	0.44	0.55
IF _{strain}	32.35 %	46.59 %	58.18 %

Figure 15 shows the effect of initial relative density D_0 on the forming load under the conditions of the area reduction of 20 %, the die semi-angle of 8° and the friction factor of 0.3. A larger value of the initial relative density would require more forming load to extrude the porous metal. The maximum forming loads approximate 28000 N, 39500 N and 49000 N for $D_0 = 0.7, 0.8$ and 0.9 , respectively. Figure 16 shows how initial relative density affects the effective stress distribution. The effective stress correlates with the distance from the centre and varies in ranges of 150-510 MPa, 230-520 MPa and 320-580 MPa for $D_0 = 0.7, 0.8$ and 0.9 , respectively. Figure 17 shows the effect of initial relative density on the effective strain distribution. The effective strain increases as the distance from the centre increases. The effective strain varies in the range of 0.21-0.425, 0.24-0.43 and 0.27-0.44 for $D_0 = 0.7, 0.8$ and 0.9 , respectively. Figure 18 shows that the initial relative density correlates positively with the relative density distribution and varies in ranges of 0.88-0.97, 0.925-0.985 and 0.975-0.995 for $D_0 = 0.7, 0.8$ and 0.9 , respectively. Table 3 shows the effect of the initial relative density on the inhomogeneous factor of effective strain. The inhomogeneity factor of effective strain correlates negatively with the reduction in area.

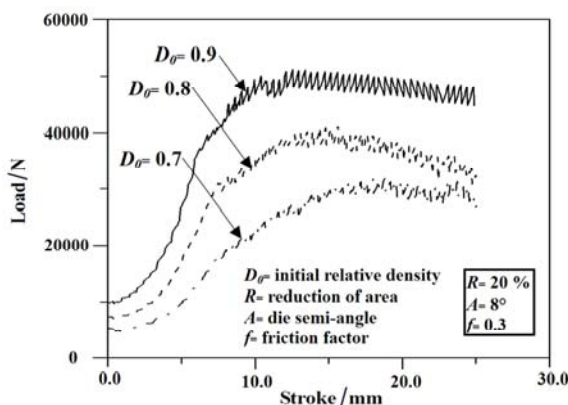


Fig. 15 Effect of initial relative density on extrusion force

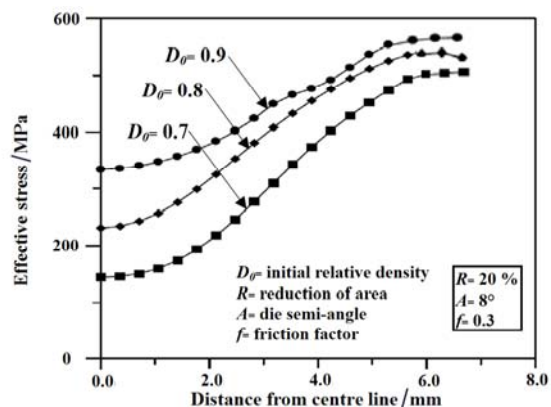


Fig. 16 Effect of initial relative density on effective stress distribution

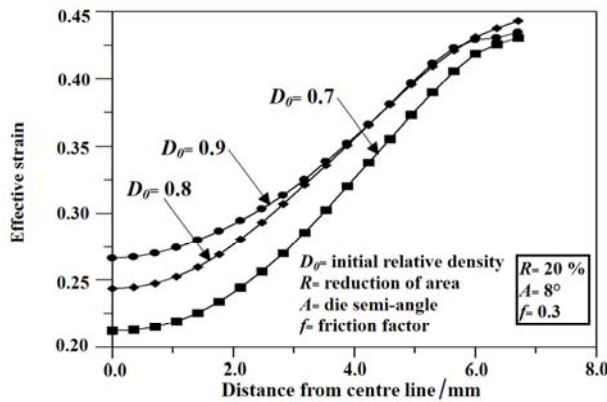


Fig. 17 Effect of initial relative density on effective strain distribution

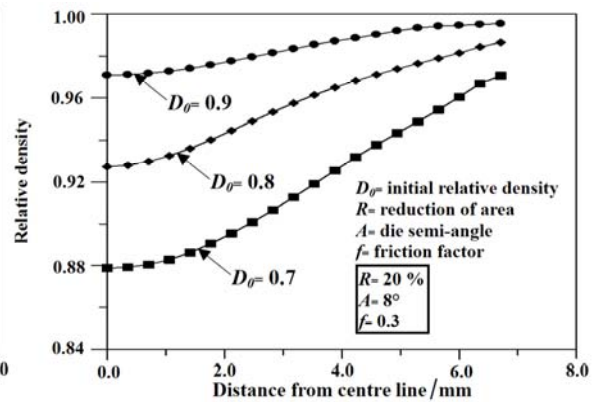


Fig. 18 Effect of initial relative density on relative density distribution

Table 3 Effect of initial relative density on the inhomogeneous factor of effective strain

Initial relative density	0.7	0.8	0.9
ϵ_c	0.21	0.24	0.27
ϵ_s	0.425	0.43	0.44
IF _{strain}	50.59 %	44.19 %	38.64 %

Figure 19 shows how friction factor f affects the forming load under the conditions of the reduction in area of 20 %, the die semi-angle of 8° and the initial relative density of 0.8. A larger value of the friction factor would require more forming load to extrude the porous metal. The maximum values of the forming load are approximately 19000 N, 39500 N and 89000 N for $f=0.1, 0.3$ and 0.5 , respectively. Figure 20 shows the effect of the friction factor on the effective stress distribution. The effective stress increases as the distance from the centre increases. The effective stress varies in ranges of 180-420 MPa, 220-540 MPa and 300-670 MPa for $f=0.1, 0.3$ and 0.5 , respectively. Figure 21 shows how friction affects the effective strain distribution. The effective strain correlates with the distance from the centre and varies in ranges of 0.19-0.35, 0.25-0.47 and 0.31-0.60 for $f=0.1, 0.3$ and 0.5 , respectively. Figure 22 shows the effect of the friction factor on the relative density distribution. The relative density correlates with the distance from the centre and varies in ranges of 0.89-0.97, 0.928-0.982 and 0.961-0.992 for $f=0.1, 0.3$ and 0.5 , respectively. Table 4 shows the effect of the friction factor on the inhomogeneous factor of effective strain. The values of the inhomogeneous factor of effective strain increase as the friction factor increases.

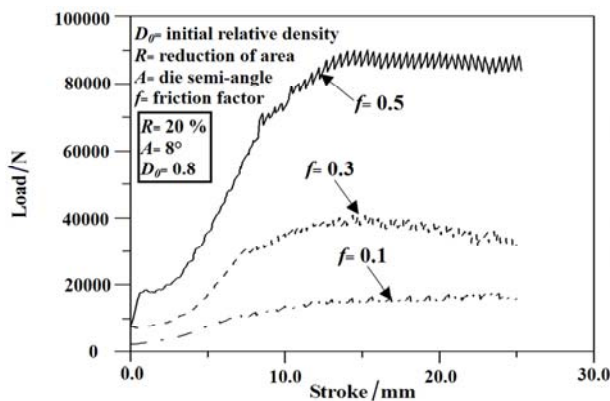


Fig. 19 Effect of friction factor on extrusion force

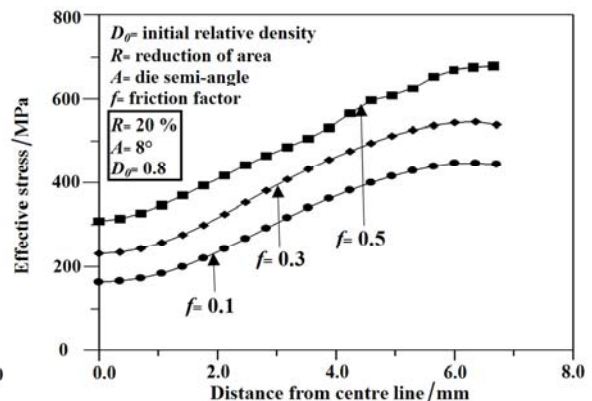


Fig. 20 Effect of friction factor on effective stress distribution

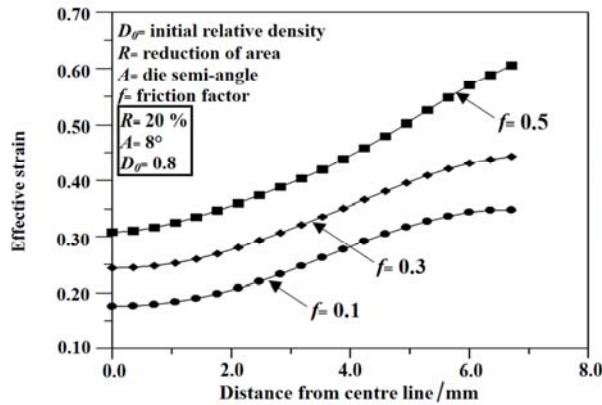


Fig. 21 Effect of friction factor on effective strain distribution

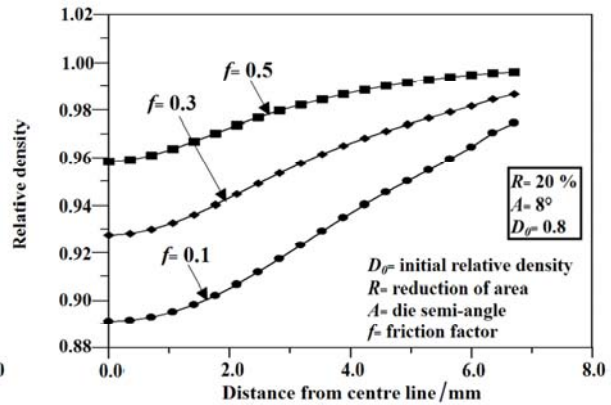


Fig. 22 Effect of friction factor on relative density distribution

Table 4 Effect of friction factor on the inhomogeneous factor of effective strain

Friction factor	0.1	0.3	0.5
ϵ_c	0.19	0.25	0.31
ϵ_s	0.35	0.47	0.60
IF _{strain}	45.71 %	46.81 %	48.33 %

4. CONCLUSIONS

In this paper, the FEM software DEFORM-2D is applied to simulate the extrusion process of porous metal. A finite element method is used to investigate the effects of forming load, effective stress distribution, relative density variation and the inhomogeneous factor of effective strain under various process parameter conditions, including the reduction in area, the die semi-angle, and the friction factor. The simulation results revealed the following:

1. The maximum forming load increases with an increase in the die semi-angle, the reduction in area, the initial relative density and the friction factor.
2. The inhomogeneous factor of effective strain increases with an increase in the die semi-angle and the friction factor. In contrast, the inhomogeneity of effective strain correlates negatively with the reduction in area and the initial relative density.
3. The effective stress, effective strain and relative density increase as the distance from the centre increases.

ACKNOWLEDGMENTS

The authors wish to thank for the support from the National Science Council of Taiwan provided under the contract NSC-96-2622-E-150-012-CC3.

REFERENCES

- [1] Khoei, A.R., Keshavarz, Sh., Khaloo, A.R.: Modeling of large deformation frictional contact in powder compaction processes, *Applied Mathematical Modelling*, 32(2008), 775-801.
- [2] Liao, K.-C.: Applications of planar anisotropic yield criteria to porous sheet metal forming simulations, *European Journal of Mechanics A/Solids*, 28(2009), 806-810.
- [3] Yang, T. S., Hsu, Y. C.: Study on the bulging deformation of the porous metal in upsetting, *Journal of Material Processing Technology*, 177(2006), 154-158.

- [4] Huang, C.C., Cheng, J.H.: Forging Simulation of Sintered Powder Compacts Under Various Frictional Conditions, *Int. J. Mech. Sci.*, 44(2002), 489-507.
- [5] DEFORM-2D User's Manual, Version 9.0, *Scientific Forming Technologies Corporation*, Ohio, 2006.
- [6] Shima, S., Oyane, M.: Plasticity Theory for Porous Metals, *Int. J. Mech. Sci.*, 18(1976), 285-291.
- [7] Lin, H.S., Hsu, Y.C., Keh, C.C.: Inhomogeneous deformation and residual stress in skin-pass axisymmetric drawing, *J. Mater. Process. Technol.*, 201(2008), 128-132.

Submitted: 25.01.2012

Accepted: 13.9.2012

Tung-Sheng Yang
National Formosa University,
Department of Mechanical and Computer-
Aided Engineering,
64, Wunhau Rd. Huwei, Yunlin 632,
Taiwan
Sheng-Yi Chang
National Formosa University,
Institute of Mechanical and Electro-
Mechanical Engineering,
64, Wunhau Rd. Huwei, Yunlin 632,
Taiwan